This is an open access article published under a Creative Commons Attribution (CC-BY) License, which permits unrestricted use, distribution and reproduction in any medium, provided the author and source are cited.

LANGMUIR

Article

pubs.acs.org/Langmuir

Mechanisms of Polymer-Templated Nanoparticle Synthesis: Contrasting ZnS and Au

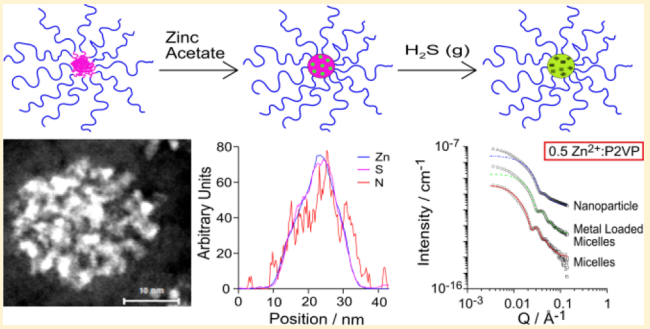
Lucia Podhorska,[†,⊥] Derfogail Delcassian,[†,⊥,§] Angela E. Goode,[†] Michael Agyei,[†,∥] David W. McComb,[†,‡] Mary P. Ryan,[†] and Iain E. Dunlop*[,†]

[†]Department of Materials, Imperial College London, Prince Consort Road, London, SW7 2AZ, United Kingdom

[‡]Department of Materials Science and Engineering and Center for Electron Microscopy and Analysis, Ohio State University, 1305 Kinnear Road, Columbus, Ohio 43212, United States

Supporting Information

ABSTRACT: We combine solution small-angle X-ray scattering (SAXS) and high-resolution analytical transmission electron microscopy (ATEM) to gain a full mechanistic understanding of substructure formation in nanoparticles templated by block copolymer reverse micelles, specifically poly(styrene)-*block*-poly(2-vinylpyridine). We report a novel substructure for micelle-templated ZnS nanoparticles, in which small crystallites (∼4 nm) exist within a larger (∼20 nm) amorphous organic−inorganic hybrid matrix. The formation of this complex structure is explained via SAXS measurements that characterize *in situ* for the first time the intermediate state of the metal-loaded micelle core: Zn^{2+} ions are distributed throughout the micelle core, which solidifies as a unit on sulfidation. The nanoparticle size is thus determined by the radius of the metal-loaded core, rather than the quantity of available metal ions. This mechanism leads to particle size counterintuitively decreasing with increasing metal content, based on the modified interactions of the metal-complexed monomers in direct contrast to gold nanoparticles templated by the same polymer.



INTRODUCTION

The ability to produce regularly spaced arrays of nanoparticles is important in a range of applications across magnetism, optics and biomaterials.[1−4] A common method is to use block copolymer spherical micelles as templates, growing nanoparticles from metal precursors localized within the micelle core. The spherical micelles can then be assembled into close-packed layers in 2D and 3D, generating materials incorporating regularly spaced highly monodisperse nanoparticles with long-range order.[5,6]

One of the most broadly applied block copolymer systems for nanoparticle synthesis is poly(styrene)-*block*-poly(2-vinylpyridine) (PS-*b*-P2VP) reverse micelles formed in simple aromatic solvents (toluene/xylene). This system has the advantage that the pyridine moieties in the poly(2-vinylpyridine) (P2VP) micelle core are readily complexed by a range of metal ions, with the nonpolar nature of the surrounding environment providing an additional driving force to localize ionic species in the core, and increase the specificity of synthesis. The PS-*b*-P2VP system has been particularly applied to gold nanoparticle synthesis, generating unique 2D nanoparticle arrays that combine sub-10 nm feature sizes with the ability to coat large areas.[7−9] This combination of properties has enabled them to be biofunctionalized to produce regular biomolecule arrays that have generated fundamental results in cell biology: determining the effect of intermolecular spacing on cell responses in biological processes including cell adhesion[10−12] and immune cell activation.[13−15] Additionally, they have been used as templates for catalyzing nanowire growth,[16] and antireflection coatings.[17] More recently, the production of nanoparticles of metal compounds has been demonstrated: oxides of iron,[18] zinc[19] and titanium[20] as well as cadmium sulfide[21] have been formed.

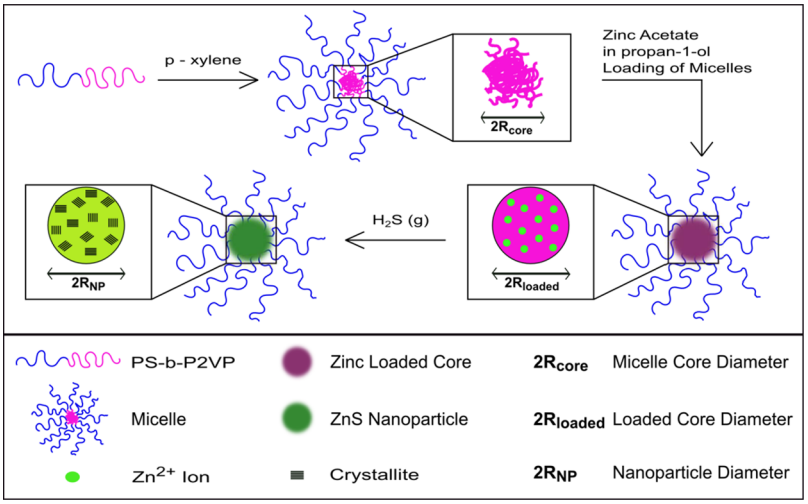
Despite the importance of the PS-*b*-P2VP templating system, the mechanisms of nanoparticle growth in these systems are not well-understood. In particular, there has been, to the best of our knowledge, no characterization of the metal-loaded micelle core in the solution state (as opposed to imaging of dried samples by TEM) despite the critical role of the metal-loaded core as an intermediate state on the route to nanoparticle formation. In the most commonly used application of gold nanoparticle synthesis, the final nanoparticles have a simple crystalline structure, and the particle volume is expected to be determined purely by the total amount of gold in each micelle,[7,22,23] and the state of the metal-loaded core may not be considered to be of high importance. However, in more complex cases, the state of the metal-loaded core may be critical in determining the final nanoparticle size and structure.

Received: May 18, 2016
Revised: August 19, 2016
Published: August 22, 2016

 © 2016 American Chemical Society

DOI: 10.1021/acs.langmuir.6b01900
Langmuir 2016, 32, 9216−9222

Scheme 1. Schematic Showing the Mechanism of ZnS Nanoparticle Synthesis: (1) Micelle Formation by Dissolution of Block Copolymer in p-Xylene, (2) Zn^{2+} Ion Encapsulation within Core of Micelles, (3) Treatment with H_2S Generated *in situ*, and (4) Formation of Single ZnS Nanoparticle with Composite Structure in Core of Micelles



In this paper, we apply block copolymer micelle templating for the first time to the synthesis of zinc sulfide (ZnS) nanoparticles. The formation of zinc sulfide nanostructures is in general somewhat complex. Specifically, ZnS tends to nucleate readily in bulk, leading to small crystallite sizes—often less than 5 nm.[24−26] In addition, such nanocrystallites have been shown to undergo postsynthesis phase transitions,[27] and to relax into a partially disordered state on exposure to solvents.[28] This complex behavior indicates a potential for interesting structures to develop during synthesis of micelle-templated nanoparticles.

To understand the mechanism of formation of micelle-templated nanoparticles with potentially complex substructure, it is necessary to apply and correlate several characterization techniques. Measuring the properties of the metal-loaded micelle core in its native solution state is ideally accomplished by synchrotron-based small-angle X-ray scattering (SAXS). SAXS is the gold standard technique (together with its neutron equivalent) to permit direct high-resolution *in situ* observation of such solution structures at room temperature and does not require complex sample preparation, using radiation of a wavelength smaller than the feature sizes.[29−32] In addition, it intrinsically averages over macroscopic numbers of particles to generate a statistically representative picture of the population. Here, we use SAXS to compare the formation of ZnS nanoparticles with the well-established case of gold nanoparticles templated by identical PS-*b*-P2VP micelles, comparing direct measurements of the metal-loaded core with the final nanoparticle in both cases.

For detailed characterization of nanoparticle structure and crystallinity, high-resolution transmission electron microscopy (HR-TEM) can be used; however, in the ZnS nanoparticle that forms within a polymer micelle, it is also necessary to map the locations of the distinct chemical components. We achieve this using energy dispersive X-ray (EDX) spectroscopy performed in the scanning transmission electron microscope (STEM), with resolution reaching ∼1 nm or better.

EXPERIMENTAL SECTION

Synthesis of PS-*b*-P2VP Templated ZnS Nanoparticles. 0.5 wt % solutions (c = 5 mg/mL) of the diblock copolymer polystyrene(x)-*block*-poly(2-vinylpyridine)(y) [PS-(x)-*b*-P2VP(y), where x, y represent the M_n of the individual chains with x = 16000, 34000, 52100, y = 3500, 18000, 31000, respectively] (Polymer Source, Inc.) dissolved in *p*-xylene (Sigma-Aldrich) were stirred overnight. For preparation of the loaded micelles, zinc acetate (Sigma-Aldrich), predissolved in propan-1-ol (Sigma-Aldrich) at 0.073 mg/μL, was added to the micelle solutions at concentrations ranging from 0.05 to 0.5:1 Zn^{2+}:P2VP ratio. The solutions were left to stir overnight. For the sulfidation of the zinc particles, the zinc acetate loaded micelle solutions were treated with H_2S generated in situ, by implementing a three-flask system: 60 mg sodium sulfide (Sigma-Aldrich) in the first flask, the Zn^{2+} micelle solution in the second, and bulk zinc nitrate (Sigma-Aldrich) in deionized water in the third. Flasks were connected and deoxygenated with nitrogen carrier gas for 10 min before 10 mL 2 M nitric acid (Sigma-Aldrich) was injected into the first flask and the reaction left to stir for 40 min. To obtain a monolayer of micelles on a surface, a previously cleaned silicon substrate was dipped into the solution and withdrawn at a constant speed. The silicon wafer was dried in air at room temperature.

Synthesis of PS-*b*-P2VP templated Au Nanoparticles. 0.5 wt % solutions (c = 5 mg/mL) of the diblock copolymer polystyrene(x)-*block*-poly(2-vinylpyridine)(y) [PS(x)-*b*-P2VP-(y), where x, y represent the M_n of the individual chains with x = 52100 and y = 31000] (Polymer Source Inc.) dissolved in *p*-xylene (Sigma-Aldrich) were stirred overnight. For preparation of the loaded micelles, gold(III) chloride hydrate (Sigma-Aldrich) was added to the micelle solutions at concentrations ranging from 0.05 to 0.5:1 Au(III):P2VP ratio. The solutions were left to stir overnight. Reduction of the gold ions to form elemental gold nanoparticles was achieved by adding hydrazine solution (1.0 M in THF) (Sigma-Aldrich) at 1:20 molar ratio of Au(III):hydrazine.

Transmission Electron Microscopy (TEM). Holey carbon coated copper TEM grids (Taab) were baked under vacuum at 120 °C for 4 h. ZnS micelle solutions were drop-cast onto TEM grids, dried in air, and imaged using a JEOL 2000FX TEM operated at 200 kV. HR-TEM imaging was carried out on an image-corrected FEI Titan 80−300 (S)TEM operated at 80 kV. Digital Micrograph (Gatan) software was used to perform Fourier transforms.

DOI: 10.1021/acs.langmuir.6b01900
Langmuir 2016, 32, 9216−9222

Dark field scanning transmission electron microscopy (STEM) imaging and EDX spectrum imaging were performed in STEM mode using a Titan^3 60−300 (FEI Company, USA) operated at 300 kV. This microscope is equipped with a high-coherence, high-brightness field emission electron gun (X-FEG) and a high-speed, high-throughput, quad-silicon drift detector (Super-X), optimized for rapid EDX collection. EDX data were postprocessed using Esprit v1.9 (Bruker Nano GmbH, Berlin, Germany) software. The incident probe size was estimated to be 0.15−0.18 nm.

Small Angle X-ray Scattering (SAXS). Data was collected on the I22 beamline at the Diamond Light Source. Fitting was carried out on the SANSVIEW program, using the built-in Sphere and Core−Shell models. Polydispersities were modeled using the Schulz distribution.

RESULTS AND DISCUSSION

Formation of ZnS Nanoparticles with Novel Hybrid Substructure. ZnS nanoparticles were synthesized in block copolymer spherical reverse micelles (PS-*b*-P2VP in *p*-xylene), with the experimental stages shown in Scheme 1 (see Experimental Section). PS-*b*-P2VP micelles were first exposed to Zn^{2+} ions via addition of zinc acetate, which is expected to lead to a *block ionomer micelle*, where the P2VP moieties that makes up the core form dative bonds to coordinate the Zn^{2+} cations.[19] The block ionomer micelles were then exposed to hydrogen sulfide gas to finally generate zinc sulfide nanoparticles; we have adapted a procedure previously reported for CdS.[21] Particles were synthesized using PS-*b*-P2VP polymers of different block molecular weights, each with two different levels of added zinc acetate corresponding to Zn^{2+}:P2VP ratios of 0.05 and 0.5. These variables controlled the overall particle size in the range 12−35 nm (see SAXS measurements below: Table 1).

Table 1. Summary of Nanoparticle Sizes As Determined by SAXS, for both ZnS and Au Nanoparticles Synthesized Using Polymer Template PS(52,100)-*b*-P2VP(31,000) with 0.05 and 0.5 Loading

polymer template	Zn^{2+}:P2VP	R_{core}/Å	Zn^{2+} R_{loaded}/Å	ZnS R_{NP}/Å
PS(52,100)-*b*-P2VP(31,000)	0.05	180	175	170
	0.5	180	135	114
polymer template	Au(III):P2VP	R_{core}/Å	Au(III) R_{loaded}/Å	Au R_{NP}/Å
PS(52,100)-*b*-P2VP(31,000)	0.05	180	180	29
	0.5	180	200	60

The structure and crystallinity of the nanoparticles was examined by HR-TEM (Figure 1). This revealed a novel composite structure, with a crystalline phase of zinc sulfide coexisting with an amorphous matrix. The crystalline phase, well-visualized using high angle annular dark-field (HAADF) STEM imaging (Figure 1C), occupies a large fraction of the nanoparticle volume, and consists of irregularly shaped nanocrystallites distributed throughout the nanoparticle. Close examination of the crystallites by bright-field HR-TEM shows a lattice fringe spacing of 0.32 nm, which is consistent with the accepted value for the (111) lattice plane in cubic spharelite ZnS,[33] and which differs from the characteristic fringe spacings in this range that would be observed from ZnO (0.26 and 0.28 nm, typical of the (002) and (100) lattice planes, respectively, of hexagonal ZnO[34]). The existence of the crystalline phase is further confirmed by the Fourier transform of the bright field (BF) image (Figure 1B), which shows a combination of bright spots associated with lattice fringes in the image and diffuse rings indicative of amorphous materials. In contrast to overall particle size, the size of crystalline features was independent of polymer block molecular weight (Figure S2, Supporting Information).

Two possible explanations for this composite structure present themselves. First, the nanoparticle could have formed by an initial precipitation of amorphous ZnS that was too rapid for the formation of the thermodynamically favored crystalline phase.[27] The crystallites could have then formed by spontaneous nucleation within an initially uniform amorphous nanoparticle (devitrification). In this case, crystallite growth would be expected to continue; however, this is not supported by observations of nanoparticles after 1 year at room temperature, which showed the crystallite size unchanged at ∼4 nm (Figure S3, Supporting Information).

The second hypothesis is that the amorphous phase is not pure ZnS, but rather a hybrid phase comprising both ZnS and P2VP. In this scenario, Zn^{2+} ions are initially distributed throughout the P2VP micelle core, complexing the pyridine moieties. Sulfidation bridges these Zn^{2+} ions without inducing phase separation, so that the P2VP is locked into the newly formed ZnS phase, clearly resulting in an amorphous structure. In specific locations where crystalline ZnS does nucleate, then crystallites can grow, but only to a size limited by the need to exclude the polymer. Alternatively, the crystallites can be explained by postulating nanometer-scale regions of high Zn^{2+} concentration within the micelle core, as has been previously proposed based on TEM observations of zinc-loaded micelles.[19]

To determine whether the amorphous phase is indeed hybrid, we performed high-resolution chemical mapping of the nanoparticle-block copolymer structure by EDX spectrum imaging. Rapid EDX collection using a large-angle EDX detector was necessary to acquire sufficient signal without imparting significant damage to the beam-sensitive organic phase of the nanoparticles. The Zn and S line profiles show the distribution of ZnS, with their colocalization in the micelle center, showing that there is no detectable zinc or sulfur, and therefore no ZnS, in the outer noncore part of the micelle (Figure 1D). Critically, the N signal shows the location of the P2VP that would have made up the micelle core prior to nanoparticle formation. This is strongly colocalized with ZnS, peaking at the center of the spherical nanoparticle. This reproduces what would be observed if the P2VP is distributed roughly evenly through the nanoparticle, and is inconsistent with the alternative scenarios of a P2VP corona around a pure ZnS sphere, which would lead to the measured intensity being greatest at the nanoparticle edges. The presence of P2VP in the nanoparticle core is thus confirmed, excluding the possibility that the amorphous phase is pure ZnS. The nature of the amorphous phase as an organic−inorganic hybrid is demonstrated by local EDX mapping, with zinc still present in significant quantities outside the crystalline regions (Figure S4, Supporting Information). Sulfur mapping similarly suggests the presence of sulfur outside the crystalline regions; however, mass loss and the lability of sulfur in response to the electron beam[35] limits the spatial resolution of EDX for these samples. The hypothesis that zinc in the nanoparticle is fully sulfided is, however, supported by the fact that the observed nanostructure did not change when the experiment was repeated with a 5×

DOI: 10.1021/acs.langmuir.6b01900
Langmuir 2016, 32, 9216−9222

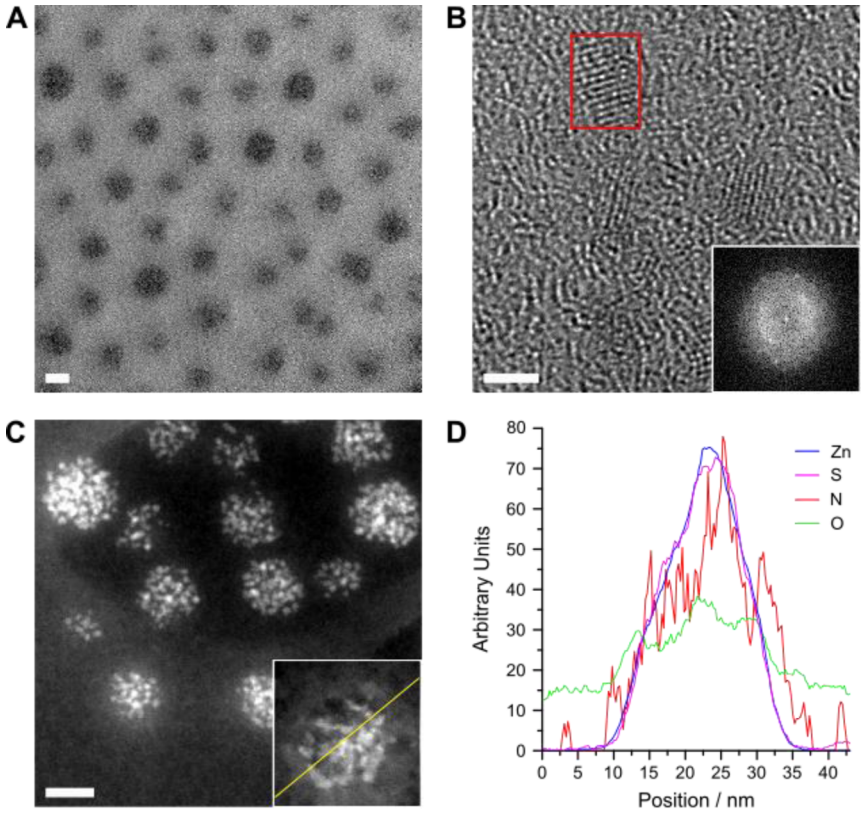


Figure 1. HR-TEM analysis of ZnS nanoparticles where (A) shows a bright field transmission electron micrograph of typical ZnS particles, synthesized using polymer template PS(52,100)-*b*-P2VP(31,000) and 0.5 loading (scale bar represents 20 nm), (B) shows a high-resolution transmission electron micrograph (HR-TEM) of ZnS crystallites of ∼4 nm diameter present in nanoparticles synthesized using the polymer template PS(52,100)-*b*-P2VP(31,000) and 0.5 loading (scale bar represents 5 nm) with an inset showing the Fourier transform containing both an amorphous ring and bright spots indicating crystallinity, (C) shows a scanning transmission electron micrograph (STEM) of nanoparticles from the same system with the inset highlighting the presence of multiple crystallites ∼4 nm in size (scale bars represent 20 and 9 nm for the main image and inset, respectively), (D) represents EDX elemental line profiles showing the amounts of Zn, S, N, and O (with each element normalized to the area under its curve) along the yellow line in the inset of panel C.

higher dose of hydrogen sulfide (Figure S3, Supporting Information). These results clearly indicate that the observed composite structure is a final structure and not a consequence of incomplete sulfidation, suggesting that the amorphous phase of the nanoparticle is indeed a P2VP-ZnS hybrid. Interestingly, based on HR-TEM images, this amorphous phase appears continuous with no other substructure (apart from the included crystalline ZnS) detectable by any method we have used.

The Intermediate State: Metal-Loaded Micelle Cores. The observed hybrid substructure of the ZnS nanoparticles has important implications for the relationship between the final nanoparticle and the intermediate state of a metal-loaded micelle. This is because the sulfidation may effectively lock the micelle core in place, so that the size and geometry of the eventual nanoparticle are likely to directly reflect those of the micelle core.

To test this conjecture, we used synchrotron small-angle X-ray scattering (SAXS) to characterize the three stages of template nanoparticle synthesis: block copolymer micelles, metal-loaded block copolymer micelles (also known as block ionomer micelles), and the final nanoparticle. SAXS profiles are shown in Figure 2 A and B (Experimental and data-fitting details in Supporting Information). To our knowledge, these are the first SAXS measurements on metal-loaded PS-*b*-P2VP micelles.

In each structure, the scattering is heavily dominated by the most electron-dense feature, which in every case can be successfully modeled as a sphere. In the case of the block copolymer micelles (Stage 1 in Scheme 1), this will be the dense micelle core, made from P2VP; detailed fitting demonstrates the expected presence of a low-density corona. In the metal-loaded micelles (Stage 2), the micelle core is predicted to comprise P2VP complexed by Zn^{2+}, leading to a much higher scattering intensity due to the electron-dense Zn. This is indeed observed (Figure 2A,B). In the final sample (Stage 3), the scattering is dominated by the ZnS nanoparticle: however, the momentum transfer range used does not permit resolution of any substructures. The radii of the micelle core, metal-loaded micelle core and nanoparticle synthesized in the PS(52,100)-*b*-P2VP(31,000) polymer template are given in Table 1.

Strikingly, it is clear that the size of the metal-loaded core does not vary greatly (Δ diameter < 3 nm) from the size of the ZnS nanoparticle. This is consistent with our proposed mechanism of formation for the nanoparticles, with the micelle core solidifying as a whole on sulfidation, trapping the P2VP to form the amorphous hybrid phase. So, the radius of the nanoparticle is essentially determined by the radius of the pre-existing metal-loaded core.

The idea that the core radius directly determines the nanoparticle radius can explain an otherwise counterintuitive

DOI: 10.1021/acs.langmuir.6b01900
Langmuir 2016, 32, 9216−9222

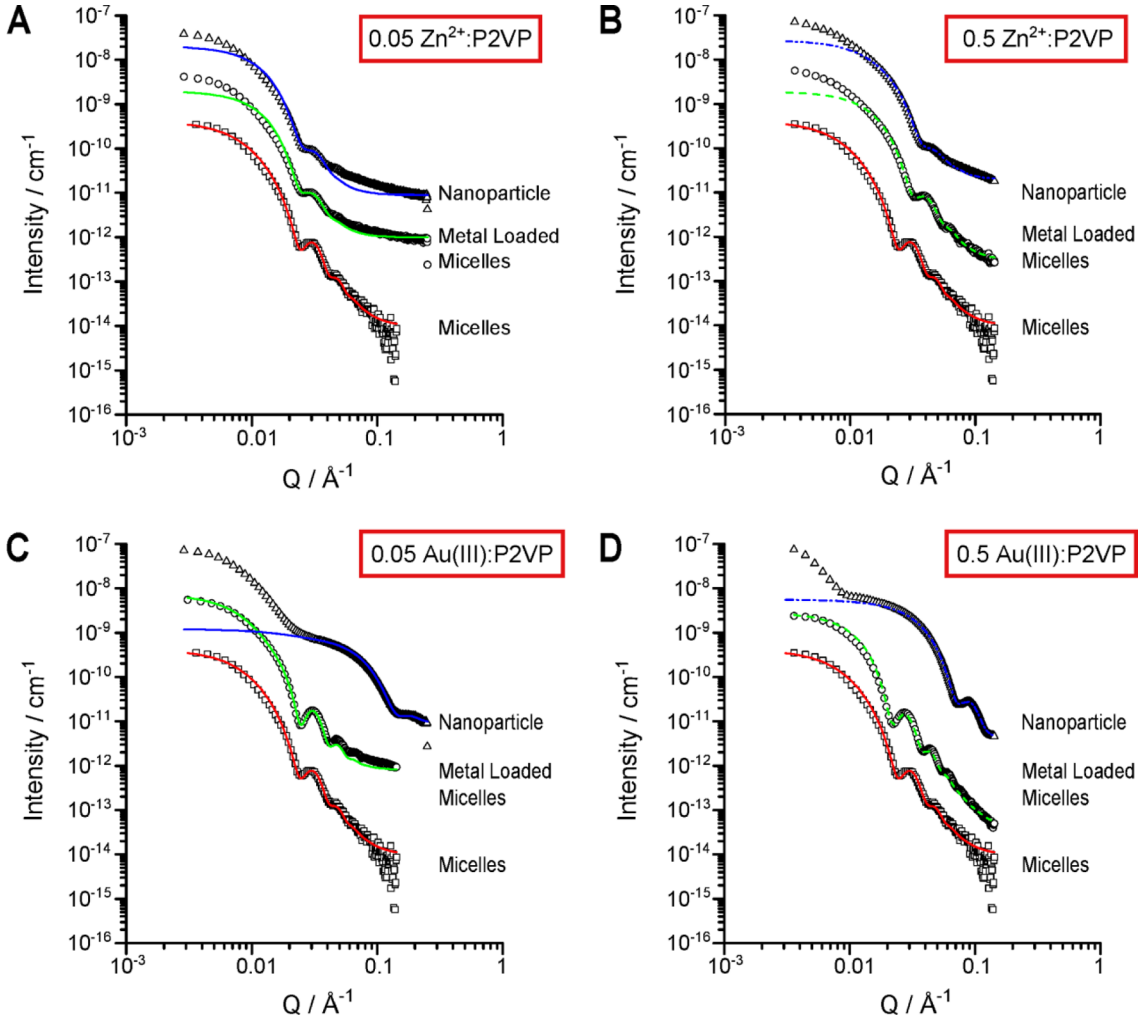


Figure 2. SAXS curves and the corresponding fitting curves for PS(52,100)-*b*-P2VP(31,000) micelles, showing the effect of loading on particle size where panel A represents 0.05 Zn^{2+}:P2VP loading concentration, and B represents 0.5 Zn^{2+}:P2VP loading concentration. The curves were vertically shifted by a constant multiplicative factor. Panel C represents 0.05 Au(III):P2VP loading, where the curves were vertically shifted by a constant multiplicative factor, and D represents 0.5 Au(III):P2VP loading ratio where only the Au loading curve was shifted by a multiplicative factor. Data was fitted to a core−shell model with a Schulz distribution and every fifth point is shown. Imperfect fitting at low Q can be attributed to the presence of small quantities of large aggregate phases in solution.

result. For the PS(52,100)-*b*-P2VP(31,000) polymer system, the nanoparticle size decreases with a substantial increase in the quantity of added zinc (Zn^{2+}:P2VP ratio 0.5 versus 0.05). This is despite the fact that the increase in metal ions added to the solution is expected to lead to an increase in the amount of metal ions in each micelle,[22,23,36,37] which in the absence of the hybrid phase would necessarily increase the nanoparticle size. Within the framework of our model, in contrast, the observation is readily explained: the lower nanoparticle size at high Zn^{2+} concentration arises from the observed change in the block ionomer micelle core size. It is expected that adding metal can decrease micelle core size, due to dipole−dipole interactions between the P2VP-Zn^{2+} complex.

Comparison of Micelle-Templated Nanoparticle Formation Mechanisms: ZnS versus Gold. The striking nature of these results confirms the distinctive formation mechanism of the ZnS composite nanoparticles. This is further illustrated by comparison with the more commonly used PS-*b*-P2VP/gold system. We have carried out for the first time SAXS measurements of gold(III) chloride ($HAuCl_4$)-loaded PS-*b*-P2VP cores, using the same polymer and metal-loading ratios as for the zinc (Figure 2C,D, Table 1). It can be seen that the size of these metal-loaded cores is not very different from the zinc. The slight increase in $HAuCl_4$-loaded core size for the 0.5 loading ratio vs the 0.05 is consistent with previous studies, which showed a direct relationship between metal loading and micelle core size.[22]

Au^{3+} reduction with hydrazine generates nanoparticles of crystalline gold as previously observed.[38,39] This can either be a single nanoparticle, if sufficiently high hydrazine concentrations are used, or controlling the rate of nucleation through hydrazine concentration can lead to the formation of multiple small nanoparticles within the micelle core.[39] SAXS measurements were performed under conditions where TEM demonstrated that single spherical nanoparticles had formed, enabling direct comparison between the radii of gold-loaded cores and nanoparticle size.

It can be seen that the gold nanoparticle radius is much less than the micelle core size in every case, in contrast to what was observed for the ZnS composite nanoparticles. This is a consequence of their pure gold composition that necessarily leads to the gold atoms occupying a much smaller volume than

DOI: 10.1021/acs.langmuir.6b01900
Langmuir 2016, 32, 9216−9222

when they were in the micellar core. Similarly, the spherical shape of the nanoparticles must arise from direct surface energy minimization and is not a consequence of the micelle core geometry as it may be in the ZnS case. Again in contrast to the ZnS, and consistent with previous studies,[8,9,23] the gold nanoparticle size increases substantially with an increase in the amount of added gold(III) chloride precursor for every polymer case. The formation of ZnS nanoparticles with the composite substructure described in this paper represents a new class of behavior beyond what has been observed so far.

SUMMARY AND CONCLUSIONS

In conclusion, we report the most detailed characterization to date of the mechanisms of formation of block copolymer micelle-templated nanoparticles. ZnS nanoparticles synthesized by templating with block copolymer (PS-*b*-P2VP) micelles show a novel composite substructure, with small (∼4 nm) regions of crystalline ZnS embedded within an amorphous hybrid matrix. SAXS characterization of the intermediate stages of synthesis shows that the nanoparticle forms by direct solidification of the metal-loaded micelle core upon sulfidation, with the final nanoparticle retaining the size of the preceding core. This stands in direct contrast to gold nanoparticles templated by the same polymer, where the nanoparticle size is determined by the total volume of gold and the rate of reduction.

ASSOCIATED CONTENT

Supporting Information

Additional characterization data. The Supporting Information is available free of charge on the ACS Publications website at DOI: 10.1021/acs.langmuir.6b01900.

(PDF)

AUTHOR INFORMATION

Corresponding Author

*E-mail: i.dunlop@imperial.ac.uk.

Present Addresses

[§]Centre for Biological Sciences, Division of Drug Delivery and Tissue Engineering, Department of Pharmacy, University Park, University of Nottingham, Nottingham, NG7 2RD, United Kingdom

[‖]St. George's Hospital, Blackshaw Road, Tooting, London, SW17 0QT, United Kingdom

Author Contributions

[⊥]These authors contributed equally.

Notes

The authors declare no competing financial interest.

ACKNOWLEDGMENTS

This work was carried out with the assistance of the DIAMOND Light Source. We thank Andrew Smith for assistance during synchrotron beamtime. I.E.D. acknowledges the funding provided by the Royal Society (RG2010/R2). L.P. would like to thank the EPSRC Doctoral Training Grant (EP/K502856/1) for financial support.

REFERENCES

(1) Bang, J.; Jeong, U.; Ryu, D. Y.; Russell, T. P.; Hawker, C. J. Block Copolymer Nanolithography: Translation of Molecular Level Control to Nanoscale Patterns. *Adv. Mater.* **2009**, *21* (47), 4769−4792.

(2) Bhaviripudi, S.; Qi, J.; Hu, E. L.; Belcher, A. M. Synthesis, Characterization, and Optical Properties of Ordered Arrays of III-Nitride Nanocrystals. *Nano Lett.* **2007**, *7* (11), 3512−3517.

(3) Ethirajan, A.; Wiedwald, U.; Boyen, H.-G.; Kern, B.; Han, L.; Klimmer, A.; Weigl, F.; Kästle, G.; Ziemann, P.; Fauth, K.; et al. A Micellar Approach to Magnetic Ultrahigh-Density Data-Storage Media: Extending the Limits of Current Colloidal Methods. *Adv. Mater.* **2007**, *19* (3), 406−410.

(4) Cheng, J. Y.; Ross, C. A.; Thomas, E. L.; Smith, H. I.; Vancso, G. J. Fabrication of Nanostructures with Long-Range Order Using Block Copolymer Lithography. *Appl. Phys. Lett.* **2002**, *81* (19), 3657.

(5) Gonçalves, M. R.; Marti, O. Experimental Observation of the Scattering of Light by Planar Metallic Nanoparticles. *New J. Phys.* **2003**, *5* (1), 160−160.

(6) Glass, R.; Arnold, M.; Blümmel, J.; Küller, A.; Möller, M.; Spatz, J. P. Micro-Nanostructured Interfaces Fabricated by the Use of Inorganic Block Copolymer Micellar Monolayers as Negative Resist for Electron-Beam Lithography. *Adv. Funct. Mater.* **2003**, *13* (7), 569−575.

(7) Glass, R.; Möller, M.; Spatz, J. P. Block Copolymer Micelle Nanolithography. *Nanotechnology* **2003**, *14* (10), 1153−1160.

(8) Lohmueller, T.; Bock, E.; Spatz, J. P. Synthesis of Quasi-Hexagonal Ordered Arrays of Metallic Nanoparticles with Tuneable Particle Size. *Adv. Mater.* **2008**, *20* (12), 2297−2302.

(9) Kästle, G.; Boyen, H.-G.; Weigl, F.; Ziemann, P.; Riethmüller, S.; Hartmann, C. H.; Spatz, J. P.; Möller, M.; Garnier, M. G.; Oelhafen, P. The Self-Organization of Metal Loaded Micelles - An Approach to Prepare Ordered Arrays of Metallic Nanoislands. *Phase Transitions* **2003**, *76* (4−5), 307−313.

(10) Shahal, T.; Geiger, B.; Dunlop, I. E.; Spatz, J. P. Regulation of Integrin Adhesions by Varying the Density of Substrate-Bound Epidermal Growth Factor. *Biointerphases* **2012**, *7* (1−4), 23.

(11) Cavalcanti-Adam, E. A.; Aydin, D.; Hirschfeld-Warneken, V. C.; Spatz, J. P. Cell Adhesion and Response to Synthetic Nanopatterned Environments by Steering Receptor Clustering and Spatial Location. *HFSP J.* **2008**, *2* (5), 276−285.

(12) Arnold, M.; Cavalcanti-Adam, E. A.; Glass, R.; Blümmel, J.; Eck, W.; Kantlehner, M.; Kessler, H.; Spatz, J. P. Activation of Integrin Function by Nanopatterned Adhesive Interfaces. *ChemPhysChem* **2004**, *5* (3), 383−388.

(13) Delcassian, D.; Depoil, D.; Rudnicka, D.; Liu, M.; Davis, D. M.; Dustin, M. L.; Dunlop, I. E. Nanoscale Ligand Spacing Influences Receptor Triggering in T Cells and NK Cells. *Nano Lett.* **2013**, *13* (11), 5608−5614.

(14) Matic, J.; Deeg, J.; Scheffold, A.; Goldstein, I.; Spatz, J. P. Fine Tuning and Efficient T Cell Activation with Stimulatory aCD3 Nanoarrays. *Nano Lett.* **2013**, *13* (11), 5090−5097.

(15) Deeg, J.; Axmann, M.; Matic, J.; Liapis, A.; Depoil, D.; Afrose, J.; Curado, S.; Dustin, M. L.; Spatz, J. P. T Cell Activation Is Determined by the Number of Presented Antigens. *Nano Lett.* **2013**, *13* (11), 5619−5626.

(16) Haupt, M.; Ladenburger, A.; Sauer, R.; Thonke, K.; Glass, R.; Roos, W.; Spatz, J. P.; Rauscher, H.; Riethmüller, S.; Möller, M. Ultraviolet-Emitting ZnO Nanowhiskers Prepared by a Vapor Transport Process on Prestructured Surfaces with Self-Assembled Polymers. *J. Appl. Phys.* **2003**, *93* (10), 6252.

(17) Lohmüller, T.; Helgert, M.; Sundermann, M.; Brunner, R.; Spatz, J. P. Biomimetic Interfaces for High-Performance Optics in the Deep-UV Light Range. *Nano Lett.* **2008**, *8* (5), 1429−1433.

(18) Yun, S.-H.; Sohn, B.-H.; Jung, J. C.; Zin, W.-C.; Ree, M.; Park, J. W. Micropatterning of a Single Layer of Nanoparticles by Lithographical Methods with Diblock Copolymer Micelles. *Nanotechnology* **2006**, *17* (2), 450−454.

(19) El-Atwani, O.; Aytun, T.; Mutaf, O. F.; Srot, V.; van Aken, P. A.; Ow-Yang, C. W. Determining the Morphology of Polystyrene-Block-poly(2-Vinylpyridine) Micellar Reactors for ZnO Nanoparticle Synthesis. *Langmuir* **2010**, *26* (10), 7431−7436.

(20) Li, X.; Lau, K. H. A.; Kim, D. H.; Knoll, W. High-Density Arrays of Titania Nanoparticles Using Monolayer Micellar Films of Diblock Copolymers as Templates. *Langmuir* **2005**, *21* (11), 5212−5217.

DOI: 10.1021/acs.langmuir.6b01900
Langmuir 2016, 32, 9216−9222

(21) Zhao, H.; Douglas, E. P.; Harrison, B. S.; Schanze, K. S. Preparation of CdS Nanoparticles in Salt-Induced Block Copolymer Micelles. *Langmuir* **2001**, *17* (26), 8428−8433.
(22) Spatz, J. P.; Sheiko, S.; Möller, M. Ion-Stabilized Block Copolymer Micelles: Film Formation and Intermicellar Interaction. *Macromolecules* **1996**, *29* (9), 3220−3226.
(23) Kästle, G.; Boyen, H. G.; Weigl, F.; Lengl, G.; Herzog, T.; Ziemann, P.; Riethmüller, S.; Mayer, O.; Hartmann, C.; Spatz, J. P.; et al. Micellar Nanoreactors—Preparation and Characterization of Hexagonally Ordered Arrays of Metallic Nanodots. *Adv. Funct. Mater.* **2003**, *13* (11), 853−861.
(24) Rath, T.; Novák, J.; Amenitsch, H.; Pein, A.; Maier, E.; Haas, W.; Hofer, F.; Trimmel, G. Real Time X-Ray Scattering Study of the Formation of ZnS Nanoparticles Using Synchrotron Radiation. *Mater. Chem. Phys.* **2014**, *144*, 310−317.
(25) Nirmala Jothi, N. S.; Joshi, A. G.; Jerald Vijay, R.; Muthuvinayagam, A.; Sagayaraj, P. Investigation on One-Pot Hydrothermal Synthesis, Structural and Optical Properties of ZnS Quantum Dots. *Mater. Chem. Phys.* **2013**, *138* (1), 186−191.
(26) Mehta, S. K.; Kumar, S.; Chaudhary, S.; Bhasin, K. K.; Gradzielski, M. Evolution of ZnS Nanoparticles via Facile CTAB Aqueous Micellar Solution Route: A Study on Controlling Parameters. *Nanoscale Res. Lett.* **2009**, *4* (1), 17−28.
(27) Barnard, A. S.; Feigl, C. A.; Russo, S. P. Morphological and Phase Stability of Zinc Blende, Amorphous and Mixed Core-Shell ZnS Nanoparticles. *Nanoscale* **2010**, *2* (10), 2294−2301.
(28) Zhang, H.; Gilbert, B.; Huang, F.; Banfield, J. F. Water-Driven Structure Transformation in Nanoparticles at Room Temperature. *Nature* **2003**, *424* (6952), 1025−1029.
(29) Dunlop, I. E.; Ryan, M. P.; Goode, A. E.; Schuster, C.; Terrill, N. J.; Weaver, J. V. M Direct Synthesis of PEG-Encapsulated Gold Nanoparticles Using Branched Copolymer Nanoreactors. *RSC Adv.* **2014**, *4* (53), 27702.
(30) Polte, J.; Erler, R.; Thünemann, A. F.; Sokolov, S.; Ahner, T. T.; Rademann, K.; Emmerling, F.; Kraehnert, R. Nucleation and Growth of Gold Nanoparticles Studied via in Situ Small Angle X-Ray Scattering at Millisecond Time Resolution. *ACS Nano* **2010**, *4* (2), 1076−1082.
(31) Abécassis, B.; Testard, F.; Spalla, O.; Barboux, P. Probing in Situ the Nucleation and Growth of Gold Nanoparticles by Small-Angle X-Ray Scattering. *Nano Lett.* **2007**, *7* (6), 1723−1727.
(32) Polte, J.; Tuaev, X.; Wuithschick, M.; Fischer, A.; Thuenemann, A. F.; Rademann, K.; Kraehnert, R.; Emmerling, F. Formation Mechanism of Colloidal Silver Nanoparticles: Analogies and Differences to the Growth of Gold Nanoparticles. *ACS Nano* **2012**, *6* (7), 5791−5802.
(33) Kremser, G.; Rath, T.; Kunert, B.; Edler, M.; Fritz-Popovski, G.; Resel, R.; Letofsky-Papst, I.; Grogger, W.; Trimmel, G. Structural Characterisation of Alkyl Amine-Capped Zinc Sulphide Nanoparticles. *J. Colloid Interface Sci.* **2012**, *369* (1), 154−159.
(34) Jiang, D.; Cao, L.; Liu, W.; Su, G.; Qu, H.; Sun, Y.; Dong, B. Synthesis and Luminescence Properties of Core/Shell ZnS:Mn/ZnO Nanoparticles. *Nanoscale Res. Lett.* **2009**, *4* (1), 78−83.
(35) Egerton, R. F.; Li, P.; Malac, M. Radiation Damage in the TEM and SEM. *Micron* **2004**, *35* (6), 399−409.
(36) Spatz, J. P.; Mössmer, S.; Hartmann, C.; Möller, M.; Herzog, T.; Krieger, M.; Boyen, H.-G.; Ziemann, P.; Kabius, B. Ordered Deposition of Inorganic Clusters from Micellar Block Copolymer Films. *Langmuir* **2000**, *16* (2), 407−415.
(37) Lu, J. Q.; Yi, S. S. Uniformly Sized Gold Nanoparticles Derived from PS-B-P2VP Block Copolymer Templates for the Controllable Synthesis of Si Nanowires. *Langmuir* **2006**, *22* (9), 3951−3954.
(38) Möller, M.; Spatz, J. P. Mineralization of Nanoparticles in Block Copolymer Micelles. *Curr. Opin. Colloid Interface Sci.* **1997**, *2* (2), 177−187.
(39) Mössmer, S.; Spatz, J. P.; Möller, M.; Aberle, T.; Schmidt, J.; Burchard, W. Solution Behavior of Poly(styrene)- B Lock -poly(2-Vinylpyridine) Micelles Containing Gold Nanoparticles. *Macromolecules* **2000**, *33* (13), 4791−4798.

DOI: 10.1021/acs.langmuir.6b01900
Langmuir 2016, 32, 9216−9222